Check for updates

NIST Technical Note
NIST TN 2238

Experimental Design for Measuring the Voltage and Current Waveforms of Appliance Usage in the NIST Net-Zero Energy Residential Test Facility

Farhad Omar, Ph.D.

This publication is available free of charge from:
https://doi.org/10.6028/NIST.TN.2238

NATIONAL INSTITUTE OF STANDARDS AND TECHNOLOGY
U.S. DEPARTMENT OF COMMERCE

NIST Technical Note
NIST TN 2238

Experimental Design for Measuring the Voltage and Current Waveforms of Appliance Usage in the NIST Net-Zero Energy Residential Test Facility

Farhad Omar, Ph.D.
Building Energy and Environment Division
Engineering Laboratory

This publication is available free of charge from:
https://doi.org/10.6028/NIST.TN.2238

September 2022

U.S. Department of Commerce
Gina M. Raimondo, Secretary

National Institute of Standards and Technology
Laurie E. Locascio, NIST Director and Under Secretary of Commerce for Standards and Technology

NIST TN 2238
September 2022

NIST Technical Series Policies
Copyright, Fair Use, and Licensing Statements
NIST Technical Series Publication Identifier Syntax

Publication History
Approved by the NIST Editorial Review Board on 2022-09-26

How to Cite this NIST Technical Series Publication
Omar F (2022) Experimental Design for Measuring the Voltage and Current Waveforms of Appliance Usage in the NIST Net-Zero Energy Residential Test Facility. (National Institute of Standards and Technology, Gaithersburg, MD), NIST Technical Note (TN) NIST TN 2238. https://doi.org/10.6028/NIST.TN.2238

NIST Author ORCID iDs
Farhad Omar: 0000-0002-0618-0060

Contact Information
farhad.omar@nist.gov

Abstract

Buildings as a set of electric loads and sources can play an essential role in managing the stability of the power system in a smart grid. Traditionally, buildings assumed a passive rule in the day-to-day operation of the electric grid. Utilities controlled the supply of energy to match the demand of buildings. However, the power distribution grid dynamics are rapidly changing due to an increase in the integration of renewable energy, electric vehicles, and non-linear loads. This technical note describes the experimental setup for measuring the voltage and current waveform data resulting from the operation of a two-stage air-source heat pump, a clothes dryer, a clothes washer, a refrigerator, a photovoltaic inverter, and a dishwasher. The experimental measurement set up is designed for the Net-Zero Energy Residential Test Facility (NZERTF) on the campus of the National Institute of Standards and Technology (NIST) in Gaithersburg, MD. Future results from this setup are intended to develop better load forecasting models and analyze the propagation of power quality issues on both sides of the utility meter while operating these appliances. This technical note also provides information about the gain and frequency response of the voltage and current sensors as well as the uncertainty of measurement.

Keywords

Current data; experimental data; experimental design; frequency response; monitoring system; sensor gains; uncertainty; voltage data.

Table of Contents

List of Tables

List of Figures

Acknowledgments

The author acknowledges the following individuals:

1. Richard L. Steiner, Ph.D., for his help and support in calibrating the voltage and current sensors used in this monitoring project and identifying the frequency response of these sensors;
2. Harrison M. Skye, Ph.D., for his help and support with the uncertainty analysis of the measurement data;
3. Mark A. Kedzierski, Ph.D., for his help and support with the uncertainty analysis of the measurement data;
4. Brian Dougherty for his help and support in measuring the electrical performance of the heat pump in the Net-Zero Energy Residential Test Facility at NIST; and
5. Glen A. Glaeser and Arthur E. Ellison for helping to install the monitoring system and capture measurements.

1. Introduction

In a smart grid, buildings can play an essential role in managing the power system's stability and quality. Traditionally, buildings assumed a passive rule in the day-to-day operation of the electric grid. Utilities controlled the supply of energy to match the demand of buildings. However, the dynamic behavior of the power distribution grid is rapidly changing. These changes are due to the integration of renewable energy sources, proliferation of electric vehicles, the increase in onsite electric storage, and a shift in the dynamic behavior of energy-consuming loads to nonlinear semiconductor-based electronics [1, 2]. The current consumption waveform of nonlinear loads is distorted and does not mimic the fundamental sinusoidal shape of the applied voltage waveform.

Studies show that building loads can be used as resources to provide ancillary services [3–5], such as voltage control and frequency regulation to maintain grid stability. In this changing environment, maintaining power quality and managing the balance between the supply and demand of electricity becomes a significant technical challenge. Resolving this technical challenge requires coordination between utility planners, aggregators, homeowners, regulators, and electricity market managers. The technical issues span various disciplines such as optimization, control theory, modeling, and simulation.

A critical aspect of managing the balance between supply and demand in the distribution grid is load forecasting [4, 6, 7]. Load forecasting requires accurate and adaptive models to account for the dynamic behavior of demand. Using load forecasting, utility planners, aggregators, and customers can devise mitigating strategies to maintain grid stability. These strategies may include controlling behind-the-meter appliances and devices by turning them on-off or shifting their operating schedules to support grid services. A critical component of load modeling is parameter identification, which broadly falls into two categories: component-based approaches and measurement-based [8]. In the component-based method, model parameters are identified from the knowledge of loads' physical behavior and the mathematical relationships that describe their characteristics. In the measurement-based approach, parameters of load models are identified from measurement data. In both categories, measurement data are vital for developing load models and validating their performances.

Maintaining power quality is another important aspect of grid operation. Power quality affects the efficiency of electrical energy consumption by end-use devices [9]. Poor power quality can lead to significant economic losses due to equipment damage, unscheduled downtime, production loss, decreased efficiency, and an unsafe work environment across all U.S. business sectors [10–12]. Power quality issues generated by individual single-phase nonlinear loads in the building sector are generally too small to cause significant distortion in the distribution grid [13], even though these issues could have a localized impact on the operating efficiency of these single-phase loads. However, as the number of these nonlinear loads increases and more buildings provide ancillary services to the grid, the cumulative power quality effect may become significant. Therefore, there is a need to investigate the impact of control actions on the cumulative response of these nonlinear loads, e.g., heat pumps.

This technical note describes the experimental approach and instrumentation used to measure the voltage and current waveforms generated by operating key appliances in the Net-Zero Energy Residential Test Facility (NZERTF) on the campus of the National Institute of Standards and

Technology (NIST) in Gaithersburg, Maryland. The NZERTF is a test facility designed with the amenities of a typical four-bedroom house in the Washington, DC metro area with a detached garage but which has much lower energy consumption than a typical home. Key features of the NZERTF related to this study are its 10 kW photovoltaic system and the use of commercially available products throughout. The exterior of the NZERTF is shown in Fig. 1 [14, 15].

Fig. 1. The NZERTF exterior

2. Experimental Approach

The overall goal of this experiment is to measure the voltage and current waveforms of key appliances at a high sample rate. High sample rate data are needed to capture the harmonic content of the waveforms. To do so, the design of the experimental setup, which is the subject of this manuscript, has the following objectives:

1. To identify appropriate voltage and current sensors;
2. To identify appropriate hardware for measuring the voltage and current waveforms and to develop the data acquisition software;
3. To identify appropriate monitoring locations for sensors placement; and
4. To characterize the gain, uncertainty, and frequency responses of the sensors.

2.1. Overall Architecture

To realize the objectives of this project, the performances of a few selected appliances were simultaneously measured at the main circuit breaker panel inside the house and on the utility side of the meter located outside of the NZERTF. Fig. **2** shows a schematic representation of the monitoring approach (top image) and the actual measurement apparatus (bottom image). It shows a typical split-phase alternating current (AC) 240 V nominal voltage configuration for distributing power in residential homes in the U.S. In this configuration, power is supplied to various loads inside the NZERTF by two live (hot) wires, designated Line 1 (L1) and Line 2

(L2). A neutral (N) wire carries the current difference between L1 and L2. In an ideal and balanced system, zero current flows through the neutral wire. The split-phase configuration supports both 240 V (line-to-line) and 120 V (line-to-neutral) loads. The L1, L2, and N cables are color-coded as black, red, and white, respectively. Installation of the ground connection (green cable) is a national electric code requirement in buildings.

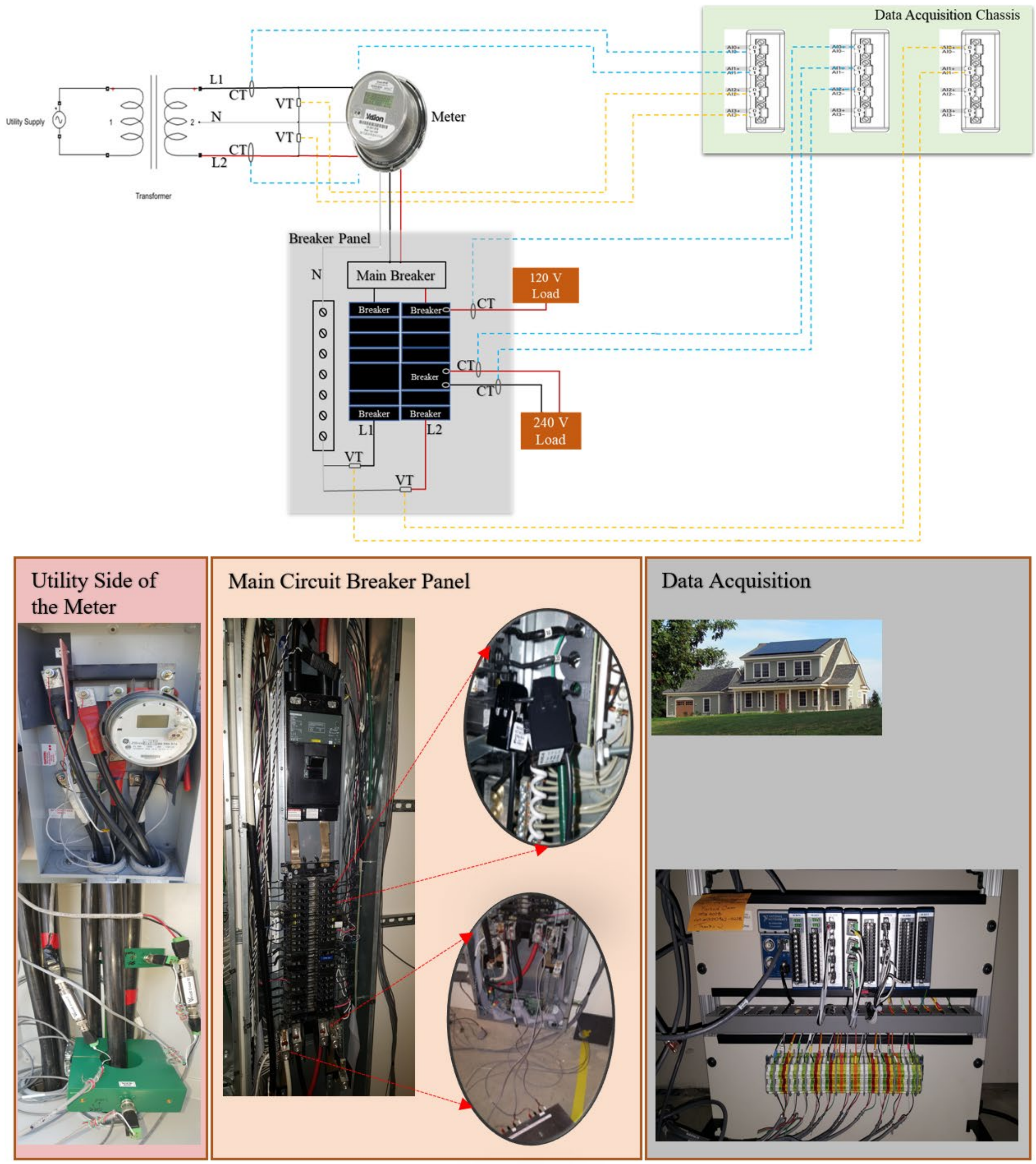

Fig. 2. A schematic representation (top image) and the actual measurement apparatus (bottom image) of the monitoring setup in the NZERTF

As shown in Fig. 2., on the utility side of the meter, two voltage sensors (VTs) and two clamp-on current sensors (CTs) were used to measure the performance of various loads in the NZERTF. The VTs measure the potential differences between the lines and the neutral (L1-N and L2-N), and the CTs measure the current flow in L1 and L2. The neutral wire is connected to the ground busbar inside the main electrical panel in residential installations. Inside the NZERTF, two VTs were used (for redundancy) on each line to measure the potential difference between the lines and the neutral or ground. To measure the current consumption on L1 and L2, one or multiple CTs, depending upon the AC voltage ratings (120 V or 240 V) of various loads, were used. A list of sensor types and their maximum ratings, functionalities, and abbreviated designations are shown in Table 1 to guide the discussion describing the measurement system. Further discussion of essential characteristics of the VTs and CTs are given in Section 1.2.1.

Table 1. Sensor Designations

Sensor Designation	Measurement Function	Type Description
CT_1	Current	Magnetic Induction (300 A root mean square (RMS))
CT_2	Current	Magnetic Induction (120 A RMS)
VT_1	Voltage	Passive voltage divider (300 V RMS)
VT_2	Voltage	Passive voltage divider (300 V, peak)
CT_3	Current	Hall-Effect (100 A RMS)
CT_4	Current	Hall-Effect (25 A RMS)
VT_3	Voltage	Active (300 V, peak)
VT_4	Voltage	Active (300 V, peak)
CT_5	Current	Hall-Effect (200 A RMS)
CT_6	Current	Hall-Effect (25 A RMS)
VT_5	Voltage	Active (300 V, peak)
VT_6	Voltage	Passive voltage divider (300 V, peak)

As shown in Table 1, there are six VTs and six clamp-on CTs. All voltage and current sensors are identified by numeric designations 1 through 6, and their outputs are scaled analog voltages of the inputs. Current sensors CT_1 and CT_2 are magnetic induction transducers. These sensors do not require external power supplies to operate. However, current sensors CT_3 to CT_6 are Hall-effect transducers. The Hall-effect sensors require an external direct current (DC) power supply to amplify their outputs. Voltage sensors, VT_1, VT_2, and VT_6, are single-ended voltage dividers. These voltage dividers measure the potential difference between a line and the ground or neutral. In residential homes, the ground and neutral wires are directly tied inside the main circuit breaker panel; therefore, all voltage measurements were conducted between lines L1 and L2 and the neutral. In this document, voltage sensors VT_1, VT_2, and VT_6 are designated passive because they do not require external power supplies to operate. However, voltage sensors VT_3, VT_4, and VT_5 are designated active because each sensor requires an external 120 V AC power supply.

Separate wiring configuration matrices (Table 2 through Table 7) were developed for each appliance to identify the location of voltage and current sensors with respect to the L1 and L2 designations. The same set of sensors listed in Table 1 were moved to different branch circuit breakers to measure the performance of each appliance. The performance of each appliance was measured in isolation to eliminate the unwanted interferences from other electrical loads; that is, all circuit breakers other than the one for the load under consideration were turned off at the main electrical panel. The following subsections describe the sensor placements to measure the electrical performances of an air-to-air heat pump, clothes dryer, clothes washer, refrigerator, photovoltaic inverter, and dishwasher.

2.1.1. Air-to-Air Heat Pump

Heating, ventilating, and air-conditioning (HVAC) is one of the largest electrical loads in a typical house. The HVAC system of the NZERTF consists of an air-source heat pump with a dedicated dehumidification cycle (available in the cooling season only) and a heat recovery ventilator (HRV) [15, 16]. The heat pump provides space conditioning while the HRV provides ventilation by bringing in fresh air. In this experiment, only the performance of the air-source heat pump was measured. The HRV unit was disconnected, and the dedicated dehumidification function of the HVAC unit was turned off.

The air-source heat pump requires a 240 V AC power supply and has two main components, an air-handling unit inside the house and an outdoor unit containing a compressor and a coil that serves as an evaporator in the heating mode and a condenser in the cooling mode. The air-handling unit uses a variable speed blower to provide conditioned air to all areas of the home. The outdoor unit utilizes a two-stage scroll compressor to provide different heating and/or cooling capacities. The sensor placement for measuring the heat pump's electrical performance is shown in Table 2.

Table 2. Sensors Placement for Measuring the Performance of the Heat Pump

Appliance \ Sensors		CT_1	CT_2	VT_1	VT_2	CT_3	CT_4	CT_5	CT_6	VT_3	VT_4	VT_5	VT_6
Meter (Utility Side of the Meter)		L1	L2	L1-N	L2-N								
Heat Pump	Air-Handling Unit					L2	L1			L2-N	L1-N	L1-N	L2-N
	Outdoor Unit							L1	L2				

As shown in Table 2, two voltage and two current sensors were used to measure the electrical performance of the heat pump on the utility side of the meter. Four CTs and four VTs were used to measure the electrical performance of the heat pump inside the NZERTF. The current consumption of the air-handling unit was measured by CT_3 and CT_4, while the current consumption of the outdoor unit was measured by CT_5 and CT_6. VT_4 and VT_5 measure voltage across the air-handling and the outdoor units on L1, and VT_3 and VT_6 measure voltage across the same air-handling and the outdoor units on L2. Each unit requires a 240 V AC power supply. Two voltage sensors were used on each line for redundancy purposes. All CTs and VTs were installed with respect to the L1 and L2 designations, as shown in Fig. 2.

2.1.2. Clothes Dryer

Like the heat pump, a typical electric residential clothes dryer requires a 240 V AC power supply. The sensor placement for measuring the electrical performance of the clothes dryers is shown in Table 3.

Table 3. Sensors Placement for Measuring the Performance of the Clothes Dryer

Sensors / Appliance	CT_1	CT_2	VT_1	VT_2	CT_3	CT_4	CT_5	CT_6	VT_3	VT_4	VT_5	VT_6
Meter (Utility Side of the Meter)	L1	L2	L1-N	L2-N								
Clothes Dryer					L2	L2	L1	L1	L2-N	L1-N	L1-N	L2-N

As shown in Table 3, two voltage and two current sensors were used to measure the clothes dryer's electrical performance on the utility side of the house meter. To measure the electrical performance of the clothes dryer inside the house, two CTs and two VTs were installed on each line, L1 and L2.

2.1.3. Clothes Washer

The clothes washer requires a 120 V AC power supply. The sensor location for measuring the electrical performance of the clothes washer is shown in Table 4.

Table 4. Sensors Placement for Measuring the Performance of the Clothes Washer

Sensors / Appliance	CT_1	CT_2	VT_1	VT_2	CT_3	CT_4	CT_5	CT_6	VT_3	VT_4	VT_5	VT_6
Meter (Utility Side of the Meter)	L1		L1-N									
Clothes Washer					L1	L1				L1-N	L1-N	

As shown in Table 4, one current and one voltage sensor were used to measure the electrical performance of the clothes washer on the utility side of the meter. Two CTs and two VTs were used on L1 inside the house to capture its electrical performance.

2.1.4. Refrigerator

The refrigerator requires a 120 V AC power supply to operate. The sensor placement for measuring the electrical performance of the refrigerator is shown in Table 5.

Table 5. Sensors Placement for Measuring the Performance of the Refrigerator

Sensors / Appliance	CT_1	CT_2	VT_1	VT_2	CT_3	CT_4	CT_5	CT_6	VT_3	VT_4	VT_5	VT_6
Meter (Utility Side of the Meter)	L1		L1-N									
Refrigerator					L1	L1				L1-N	L1-N	

As shown in Table 5, one current and one voltage sensor were used to measure the electrical performance of the refrigerator on the utility side of the meter. Two CTs and two VTs were used on L1 inside the house to capture its electrical performance.

2.1.5. Photovoltaic Inverter

There are two (5 kW) grid-tied photovoltaic inverters in the attic of the NZERTF [15]. Each inverter provides single-phase 240 V AC; however, their outputs are combined into one unit within a distribution panel in the attic of the NZERTF. The output from the distribution panel is connected to the NZERTF’s main electrical panel in the basement, where the voltage and current generation of the inverter system were measured. The sensor placement for measuring the electrical performance of the inverter is shown in Table 6.

Table 6. Sensors Placement for Measuring the Performance of the Photovoltaic Inverter

Sensors / Appliance	CT_1	CT_2	VT_1	VT_2	CT_3	CT_4	CT_5	CT_6	VT_3	VT_4	VT_5	VT_6
Meter (Utility Side of the Meter)	L1	L2	L1-N	L2-N								
Photovoltaic Inverter					L2	L1			L2-N	L1-N	L1-N	L2-N

As shown in Table 6, two current and two voltage sensors (VT_1 and VT_2) were used to measure the electrical performance of the inverter on the utility side of the meter. Two CTs, one on each line L1 and L2, and four VTs, two on each line L1 and L2, were used inside the main breaker panel to capture the electrical performance of the two inverters after they are combined in distribution panel.

2.1.6. Dishwasher

The dishwasher requires a 120 V AC power supply to operate. Sensor placement for measuring the electrical performance of the dishwasher is shown in Table 7.

Table 7. Sensors Placement for Measuring the Performance of the Dishwasher

Sensors / Appliance	CT_1	CT_2	VT_1	VT_2	CT_3	CT_4	CT_5	CT_6	VT_3	VT_4	VT_5	VT_6
Meter (Utility Side of the Meter)		L2		L2-N								
Dishwasher					L2			L2		L2-N	L2-N	

As shown in Table 7, one current and one voltage sensor were used to measure the electrical performance of the dishwasher on the utility side of the meter. Inside the house, two CTs and two VTs were used on L2 to capture the electrical performance of the dishwasher.

2.2. Data Acquisition

Three analog input cards and a data acquisition chassis were used to measure the output of all voltage and current sensors. The manufacturer’s specifications for the analog cards are tabulated in Table 8.

Table 8. Manufacturer Provided Characteristics of the Analog Input Cards

Measurement Cards	Measurement Range	Number of Channels	Bandwidth	Channel Type	Input Type	Simultaneous Sample Rate	Precision
Card 1	± 10 V (VDC, VAC Peak)	4	1 MHz	Differential	Analog	1 MS/s/ch	16-bit
Card 2	± 10 V (VDC, VAC Peak)	4	0.5 MHz	Differential	Analog	0.5 MS/s/ch	16-bit

As shown in Table 8, all analog cards have an input range of ± 10 V, four differential input channels, and a bandwidth of at least 0.5 MHz to support high sample rates of the voltage and current waveforms to capture harmonic frequencies. Fig. **3** shows an image of the measurement apparatus used in this experiment.

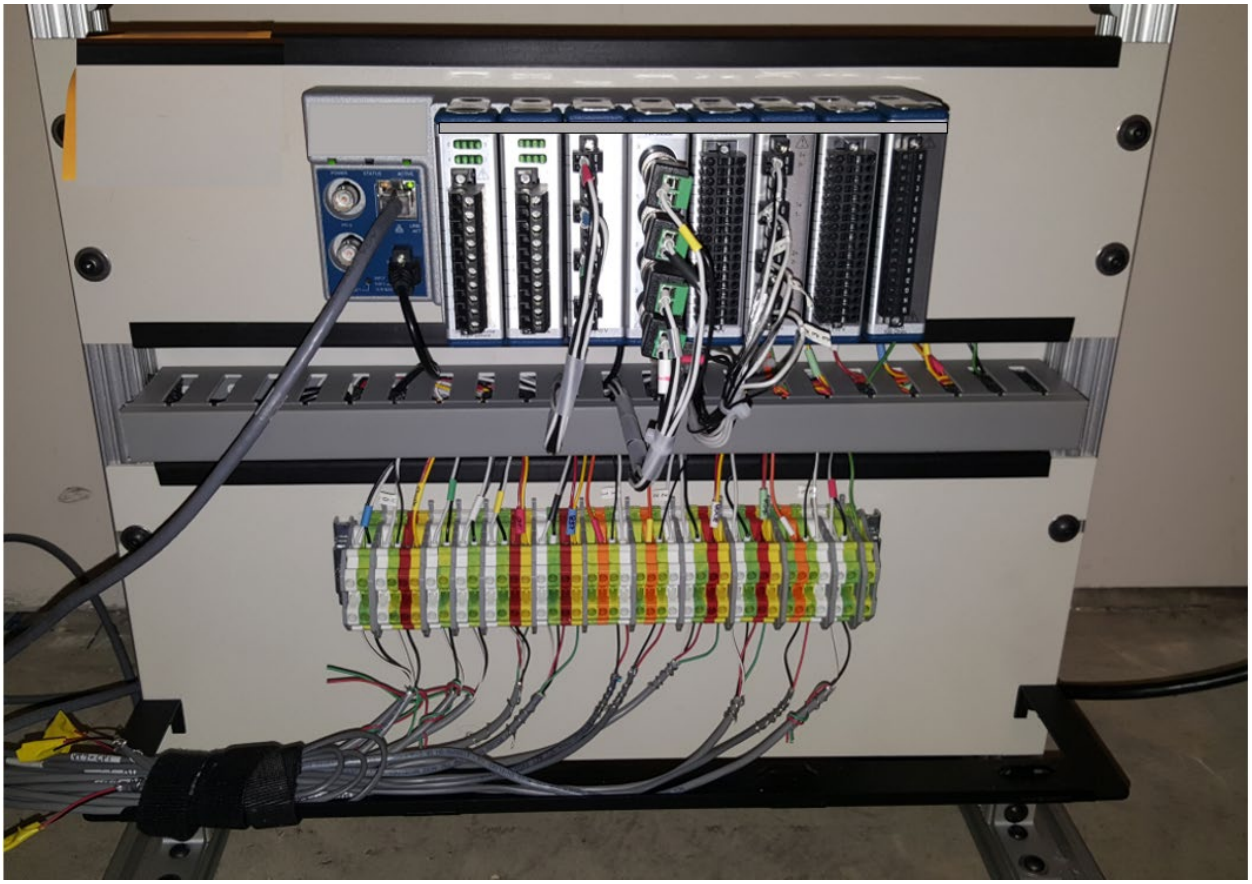

Fig. 3. The data acquisition chassis and analog cards

The data acquisition chassis was connected to a laptop computer via an Ethernet cable. Custom developed LabVIEW software was used to collect and record measurement data.

2.2.1. Overview of Sensors

This section summarizes the key characteristics of the voltage and current sensors used in this study. These characteristics are obtained from the manufacturers' technical datasheets or websites. The key considerations in selecting these sensors were their rated outputs, input current or voltage limits, accuracy, and bandwidth sufficient to capture harmonic frequencies. The sensing mechanisms of these sensors were introduced in Table 1.

Table 9 shows the current rating in RMS, measurement sensitivity, and bandwidth of the magnetic induction CTs.

Table 9. Manufacturer Provided Characteristics of the Magnetic Induction CTs

Sensor Designation	Rated Maximum RMS Current (A)	Sensitivity of Measured Current	Bandwidth
CT_1	300	0.01 V/A + 1%	1.5 Hz to 2 MHz
CT_2	125	0.01 V/A + 1%	5 Hz to 2 MHz

Table 10 shows the input current RMS ratings, accuracy, maximum offset voltage, and bandwidth of the hall-effect CTs.

Table 10. Manufacturer Provided Characteristics of the Hall-Effect CTs

Sensor Designation	Rated Current (A)	Output at Rated Current (± V)	± Uncertainty (A)	Offset Voltage (± mV)	Bandwidth
CT_3	100	4 (AC or DC)	1	100 mV max, 30 mV max for 50 Amp and up	167 kHz
CT_4	25	4 (AC or DC)	0.25	100 mV max	167 kHz
CT_5	200	4 (AC or DC)	2	20 mV max	167 kHz
CT_6	25	4 (AC or DC)	0.25	100 mV max	167 kHz

Table 11 shows the input voltage rating, accuracy, maximum output voltage, and bandwidth of the passive VTs.

Table 11. Manufacturer Provided Characteristics of the Passive VTs

Sensor Designation	Rated Voltage (V)	Output Voltage (±V)	± Uncertainty (V)	Bandwidth
VT_1	300 (RMS)	2	1.5	50 MHz
VT_2	300 (Peak-Peak)	10	0.6	85 kHz
VT-6	300 (Peak-Peak)	10	0.6	85 kHz

Table 12 shows the input voltage RMS ratings, accuracy, maximum output voltage, and bandwidth of the active VTs.

Table 12. Manufacturer Provided Characteristics of the Active VTs

Sensor Designation	Rated Voltage (V) (Peak-Peak)	Output Voltage (±V)	± Uncertainty (V)	Bandwidth
VT_3	300	10	0.75	10 kHz
VT_4	300	10	0.75	10 kHz
VT_5	300	10	0.75	10 kHz

All sensors were calibrated to characterize their electrical performance, enabling us to better estimate their measurement uncertainties. Table 13 and Table 14 show the calibrated gain and the total expanded uncertainty of all sensors used to measure the electrical performance of the loads reported in Section 1.1. The expanded uncertainty is reported with a coverage factor of $k = 2$ (95 % confidence level). Table 13 shows the calibrated gain and the uncertainty of all CTs used in this study. The output of each CT is a scaled-down AC voltage corresponding to the AC input current signal. The gain of each sensor converts the output of the CTs back to the actual nominal AC current consumption levels. The calibrated uncertainty is applicable when the RMS values of the current consumption are computed from the waveform data. For example, let CT_1 capture one second of the current consumption waveform. Then the RMS value calculated from the one-second waveform data will have an uncertainty of ± 0.14 A at a 95 % confidence level.

Table 13. Calibrated Gain and Uncertainty of CTs

Sensor Designation	Gain (A/V)	± Uncertainty (A)
CT_1	99.58	0.14
CT_2	100.00	0.14
CT_3	24.87	0.16
CT_4	6.33	0.20
CT_5	49.29	0.10
CT_6	6.39	0.11

Table 14 shows the calibrated gain and uncertainty of all VTs used in this study. The output of each VT is a scaled-down version of the AC input voltage in volts. The gain of each sensor helps us convert the output of the VTs back to the actual voltage levels. The calibrated uncertainty is applicable when the RMS values of the voltage are computed from the waveform data.

Table 14. Calibrated Gain and Uncertainty of VTs

Sensor Designation	Gain (V/V)	± Uncertainty (V)
VT_1	149.63	0.35
VT_2	29.22	0.01
VT_3	29.99	0.06
VT_4	30.02	0.11
VT_5	30.00	0.08
VT_6	29.22	0.01

The outputs of the VTs and CTs were connected to the analog cards via twisted-pair cables. The length of the wires carrying the output voltage signals from various sensors to the data acquisition system was approximately 19 m (65 ft), which introduces an impedance mismatch between the outputs of the sensors and the analog inputs of the data acquisition cards. The resulting impedance mismatch can effectively act as a filter, degrading the magnitude of the acquired signal as a function of frequency. The implication of the impedance mismatch on the frequency response of VTs and CTs is discussed in Section 1.2.1.1.

2.2.1.1. Frequency Response

An important aspect of performing quantitative analyses, such as finding the RMS of voltage and current or analyzing harmonic distortion, is understanding data quality. The quality of a data set depends on many factors, such as sample rate, accuracy and resolution of the sensors, uncertainty of the analog to digital conversion in data acquisition unit, uncertainty of measurand, and the frequency response of sensors. This section discusses the frequency response of the voltage and current sensors; other characteristics of sensors were introduced in Section 1.2.1.. The frequency response of a sensor is not only a function of its bandwidth but also the impedance match between its output and the input of the data acquisition unit. Other environmental effects include electromagnetic background noise and temperature, which can influence the quality of the measured data.

The frequency responses of the VTs and CTs used in this experiment were measured in a laboratory using a calibrator unit as a source for generating voltage and current waveforms. At the calibrator unit, the amplitudes of the voltage and current waveforms were maintained at constant values. However, the frequency of the generated signals was changed over a range of values from 60 Hz to 100 kHz. Measuring the generated waveforms, the VTs and CTs were connected to the data acquisition unit using the same twisted-pair cable as the wires used in the actual experiment to collect the voltage and current waveforms in the NZERTF. The VTs were tested using two different lengths of twisted-pair wires. The lengths of the cables were approximately 1.8 m (6 ft) and 10.7 m (35 ft), respectively. However, the CTs were tested only using one length of 1.8 m (6 ft) of twisted-pair cables. The frequency responses of representative VTs and CTs are shown in Fig. 4, Fig. 5, and Fig. 6. Sensors with the same electrical characteristics as those that appear in the figures are not shown.

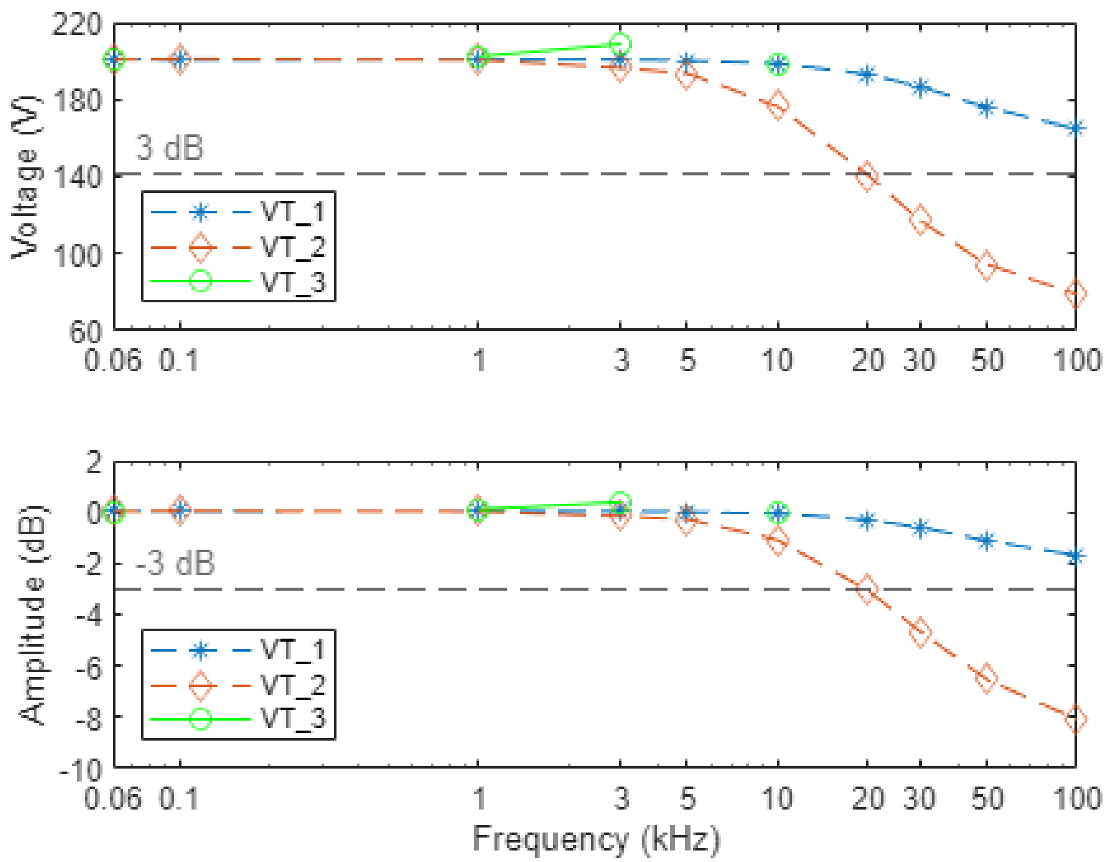

Fig. 4. Frequency response of voltage sensors using 1.8 m long twisted-pair cables between the output of the sensors and the inputs of the data acquisition equipment

The top image in Fig. 4 shows the RMS amplitude of the voltage sensors as a function of frequency, while the bottom image shows the same data, but the y-axis is presented in units of decibel. The x-coordinate frequencies are plotted using a base-10 logarithmic scale. As shown in Fig. 4, VT_1 and VT_3 exhibit similar behavior up to 10 kHz, while VT_2 starts to diverge after the 3 kHz mark.

The VT_3 sensor has a 10 kHz bandwidth; therefore, data beyond its rated frequency were not collected. In general, the amplitude of the RMS voltages for both VT_1 and VT_2 attenuated at higher frequencies. However, the amplitude of the VT_2 sensor attenuates beyond the -3 dB bandwidth at approximately 20 kHz. The -3 dB drop in the voltage magnitude means that the voltage RMS amplitude is reduced to 0.707 (about 30 %) of its peak (nominal) value, and the voltage and current signal's power in the frequency domain is reduced by 50 %.

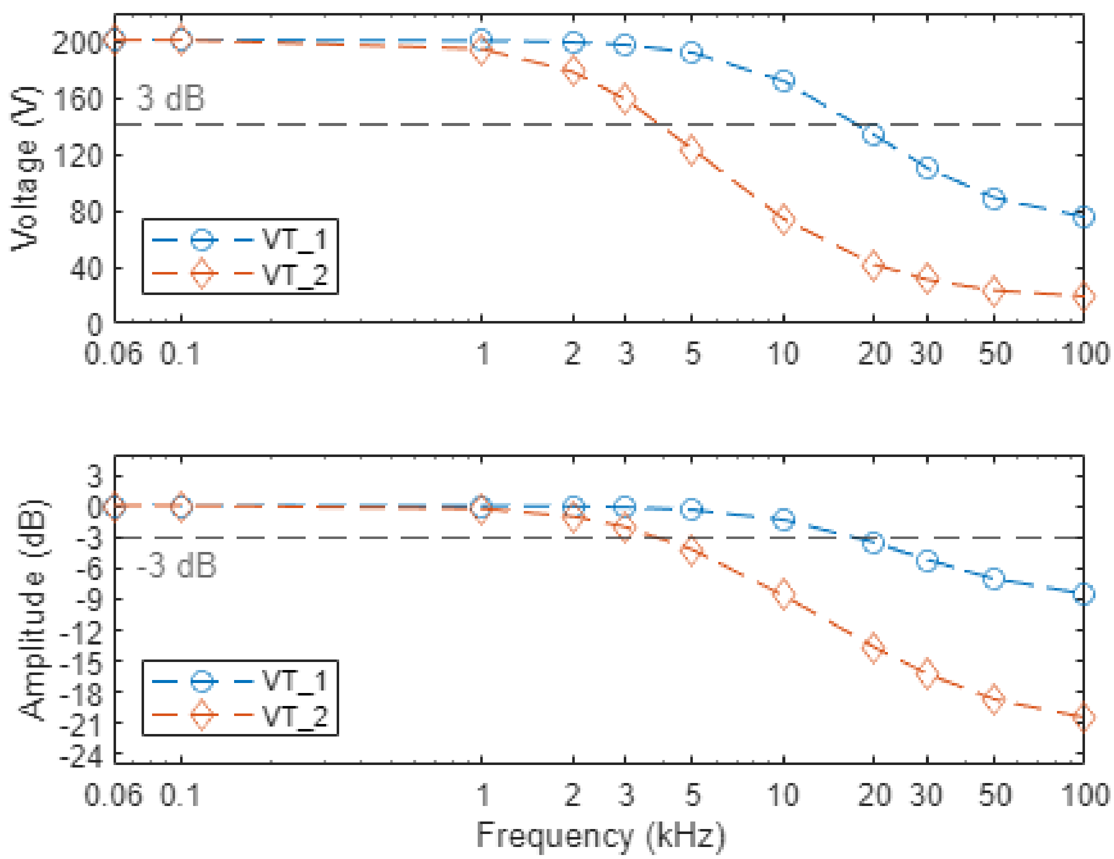

Fig. 5. Frequency response of voltage sensors using 10.7 m long twisted-pair cables between the output of the sensors and the inputs of the data acquisition equipment

Fig. 5 shows the frequency response of the voltage sensors using 10.7 m long twisted-pair cables. The top image in Fig. 5 shows the RMS amplitude of the voltage sensors as a function of frequency, while the bottom subplot shows the same data, but with the y-axis data presented in decibels. The x-coordinate frequencies are plotted using a base-10 logarithmic scale.

As shown in Fig. 5, both VT_1 and VT_2 exhibit a sharp drop in the value of the RMS voltages beyond the -3 dB bandwidth at lower frequencies compared to the data shown in Fig. 4. VT_3 sensor was not tested for this configuration. In Fig. 4, VT_1 never crossed the -3 dB bandwidth; however, with the longer cable, its amplitude attenuated beyond the -3 dB bandwidth at approximately 18 kHz, as shown in Fig. 5. Likewise, the frequency response of VT_2 shows that its amplitude decayed beyond the -3 dB bandwidth at approximately 4 kHz. The frequency responses of VT_1 and VT_2 were not measured with cable lengths longer than 10.7 m.

Fig. 6 shows the frequency responses of current sensors using 1.8 m long twisted-pair cables between the sensors' output and the data acquisition equipment inputs. The frequency responses of the current sensors beyond 10 kHz and using longer twisted-pair cables were not measured.

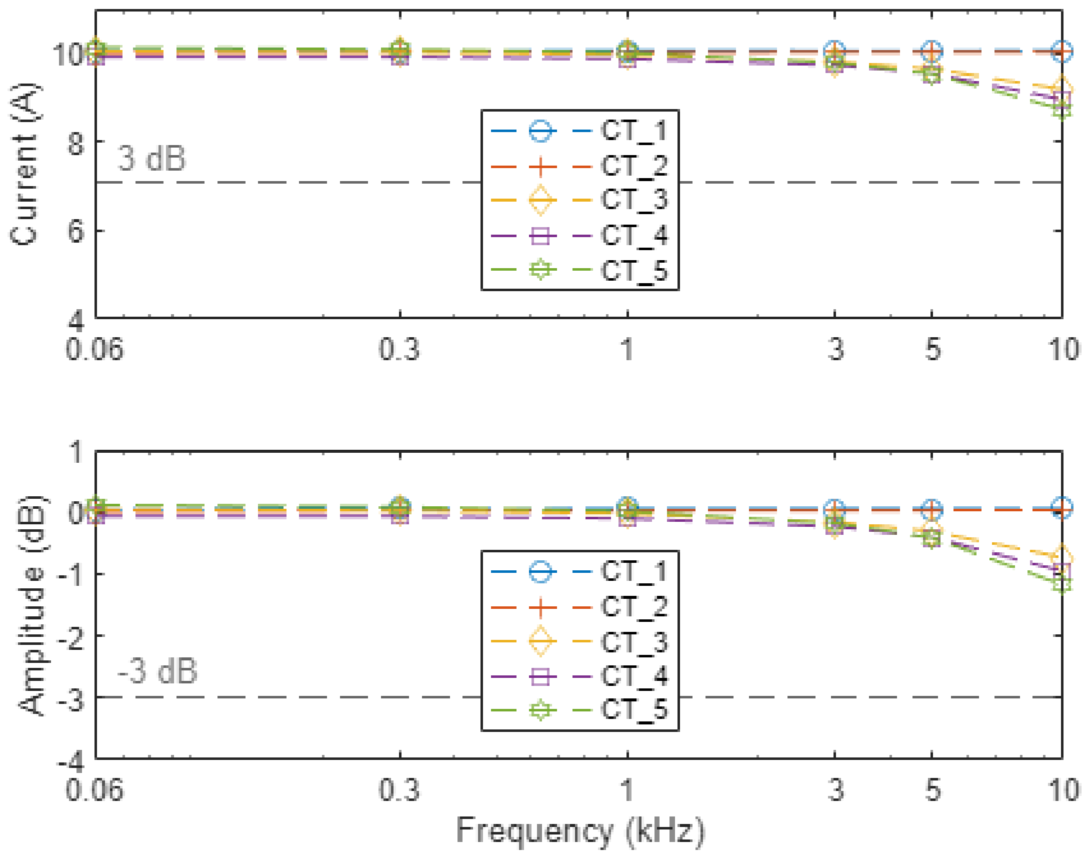

Fig. 6. Frequency response of current sensors using 1.8 m long twisted-pair cables between the output of the sensors and the inputs of the data acquisition equipment

As shown in Fig. 6, the frequency responses of all CTs remain well above the -3 dB bandwidth. However, it is assumed that the frequency response of the CTs will further attenuate as the lengths of the cables carrying the output of the sensors to the data acquisition equipment are extended beyond 1.8 m. The frequency responses of CT_1 and CT_2 sensors do not exhibit any degradation in the RMS current amplitude from the nominal 10 A peak. The remaining CTs show a downward trend toward the -3 dB bandwidth line after 1 kHz.

In the actual experiment, the cables were longer than 10.7 m. The twisted-pair wires carrying voltage and current measurements from the utility side of the meter (Fig. 2) to the data acquisition equipment in the basement of the NZERTF were approximately 21.3 m (70 ft) long. Similarly, the twisted-pair cables carrying voltage and current measurements from the main circuit breaker panel (Fig. 2) to the data acquisition equipment were approximately 21.3 m (70 ft) long. Based on the frequency responses of the sensors, the information in Table 15 serves as a guide for utilizing the data set collected in this experiment. Table 15 shows the types of analyses supported by the data set and the recommended range of frequencies for performing harmonic distortion analysis. The data from the sensors will be used to calculate the RMS values of the voltage and current, power factor, real and reactive power, and to develop appliance load models.

Table 15. Available Frequency Ranges for Harmonic Analysis

Sensor Designations	Harmonics Analysis Frequency Range
VT_1	60 Hz to 5 kHz
VT_2, VT_6	60 Hz to 3 kHz
VT_3, VT_4, VT_5	60 Hz to 1 kHz
CT_1, CT_2	60 Hz to 5 kHz
CT_3, CT_4, CT_5, CT_6	60 Hz to 3 kHz

3. Conclusion and Future Work

This technical note describes the experimental approach and instrumentation used to measure voltage and current waveforms to characterize the electrical performance of essential appliances in the NZERTF. The procedure described in this document was developed to meet the study's overall objectives:

1. Developing load forecasting models;
2. Analyzing the propagation of power quality issues, e.g., harmonics on both sides of the utility meter; and
3. Analyzing the cumulative effect of controlling key end-use appliances on power quality and stability of the distribution grid.

This document also summarizes critical characteristics of the voltage and current sensors and their gain and uncertainties. It provides critical insights into the frequency responses of the sensors and a guide for applying the data set. The outcomes of the modeling exercise and harmonic distortion analysis are the subjects of future publications.

References

[1] NIST (2021) NIST Framework and Roadmap for Smart Grid Interoperability Standards, Release 4.0. *NIST Special Publication 1108r4* https://doi.org/https://doi.org/10.6028/NIST.SP.1108r4

[2] Schwartz L, Leventis G, Zetterberg J (2020) Grid-Interactive Efficient Buildings: An Introduction for State and Local Governments FOR MORE INFORMATION Regarding Grid-interactive Efficient Buildings: An Introduction for State and Local Governments, please contact. (April). Available at www.seeaction.energy.gov

[3] Lee ZE, Sun Q, Ma Z, Wang J, MacDonald JS, Max Zhang K (2020) Providing Grid Services With Heat Pumps: A Review. *ASME Journal of Engineering for Sustainable Buildings and Cities* 1(1):1–11. https://doi.org/10.1115/1.4045819

[4] U.S. Department of Energy (2011) Load Participation in Ancillary Services. Available at https://www1.eere.energy.gov/analysis/pdfs/load_participation_in_ancillary_services_workshop_report.pdf

[5] Holmberg D, Omar F (2018) Characterization of Residential Distributed Energy Resource Potential to Provide Ancillary Services. *NIST Special Publication 1900-601*:36. Available at https://doi.org/10.6028/NIST.SP.1900-601

[6] Fuller JC, Vyakaranam BGNVSR, Kumar NP, Leistritz SM, Parker GB (2012) Modeling of GE Appliances in GridLAB-D: Peak Demand Reduction. (PNNL-21358):157. Available at http://www.pnnl.gov/main/publications/external/technical_reports/PNNL-21358.pdf

[7] Fischer D, Madani H (2017) On heat pumps in smart grids: A review. *Renewable and Sustainable Energy Reviews* 70(November 2016):342–357. https://doi.org/10.1016/j.rser.2016.11.182

[8] Arif A, Wang Z, Wang J, Mather B, Bashualdo H, Zhao D (2018) Load modeling - A review. *IEEE Transactions on Smart Grid* 9(6):5986–5999. https://doi.org/10.1109/TSG.2017.2700436

[9] Michalec Ł, Jasiński M, Sikorski T, Leonowicz Z, Jasiński Ł, Suresh V (2021) Impact of harmonic currents of nonlinear loads on power quality of a low voltage network—review and case study. *Energies* 14(12). https://doi.org/10.3390/en14123665

[10] Lineweber, D. and McNulty S (2001) The Cost of Power Disturbances to Industrial & Digital Economy Companies. *EPRI* Available at https://www.epri.com/research/products/3002000476

[11] Sharma A, Rajpurohit BS, Singh SN (2018) A review on economics of power quality: Impact, assessment and mitigation. *Renewable and Sustainable Energy Reviews* 88(May 2016):363–372. https://doi.org/10.1016/j.rser.2018.02.011

[12] Bhattacharyya S, Myrzik JMA, Kling WL (2007) Consequences of poor power quality - An overview. *Proceedings of the Universities Power Engineering Conference* (1):651–656. https://doi.org/10.1109/UPEC.2007.4469025

[13] Mansoor A, Grady WM, Chowdhury AH, Samotyj MJ (1995) An Investigation of Harmonics Attenuation and Diversity Among Distributed Single-phase Power Electronic Loads. *IEEE Transaction on Power Delivery* 10(1):6–12. https://doi.org/10.1109/61.368365

[14] Omar F, Bushby ST (2013) Simulating Occupancy in The NIST Net-Zero Energy Residential Test Facility. *NIST Technical Note 1817*. https://doi.org/https://doi.org/10.6028/NIST.TN.1817

[15] Davis M, Healy W, Boyd M, Ng L, Payne V, Skye H, Ullah T (2004) Monitoring Techniques for the Net-Zero Energy Residential Test Facility. *NIST Technical Note 1854*. Available at http://dx.doi.org/10.6028/NIST.TN.1854

[16] Fanney H, Payne V, Ullah T, Lisa N, Boyd M, Omar F, Davis M, Skye H, Dougherty B, Polidoro B, Healy W, Kneifel J, Pettit B (2015) Net-zero and Beyond! Design and Performance of NIST's Net-zero Energy Residential Test Facility. *Energy and Buildings 101*:95–109. https://doi.org/http://dx.doi.org/10.1016/j.enbuild.2015.05.002